International Journal of the Korean Society of Precision Engineering Vol. 3, No. 2, April 2002.

Synchronous Vibration Control of a Rigid Rotor System using Active Air Bearing

Tae-Kyu Kwon[1], Jin-Hao Qiu[2], Jun-JI Tani[2], and Seong-Cheol Lee[1]

[1]Department of Mechanical Engineering(RIIT), Chonbuk National University, Jeonju, 561-756 Korea
[2]Department of Mechanical Engineering, Tohoku University, Sendai, 980-8579 Japan

ABSTRACT

This paper presents the synchronous vibration control of a rotor system using an Active Air Bearing(AAB). In order to suppress the synchronous vibration, it is necessary to actively control the air film pressure or the air film thickness. In this study, active pads are used to control the air film thickness. Active pads are supported by the pivots containing piezoelectric actuators and their radial positions can be actively controlled by applying voltage to the actuators. Disturbances and various kinds of external forces can cause the shaft vibration as well as the change of the air film thickness. The dynamic behaviors of a rotary system supported by two tilting-pad gas bearings and its active stabilization using the tilting-pads as actuators are investigated numerically. The PID controller is applied to the tilting-pad gas bearing system with three pads, two of which contain piezoelectric actuators. To test the validity of the theoretical method, the performance of this control method is evaluated through experiments. The experimental results show the effectiveness of the control system for suppressing the unbalanced response of the rigid modes.

Key Words : Active air bearing, Active pad, Gas expander, Synchronous vibration, Active control.

Nomenclature

$A_j = R\alpha_i/\mu$ (j=1, 2)

c_{xx}, c_{xy}, c_{yx}, c_{yy} = damping coefficients

C = dimensionless stiffness coefficients($= cC_r/p_aR^2$)

C_{xx}, C_{xy}, C_{yx}, C_{yy} = dimensionless damping coefficients

$C_{mxx} = C_{xx}R/I_t\omega^2$, $C_{mxy} = C_{xy}R/I_t\omega^2$

$C_{myx} = C_{yx}R/I_t\omega^2$, $C_{myy} = C_{yy}R/I_t\omega^2$

C_p = friction coefficient of pivot

C_r = bearing clearance(μm)

$D = p_aR^4/JC_r\Omega^2$

h = air thickness between shaft and pad

H = dimensionless thickness ($= h/C_r$)

i = index of pad number(i=1,2,3)

I_t, I_p = moment of inertia, polar moment of inertia

j = index of bearing number(j=1,2)

J = inertia moment of a pad

k_{xx}, k_{xy}, k_{yx}, k_{yy} = stiffness coefficients

K = dimensionless stiffness coefficients($= kC_r/p_aR^2$)

K_{xx}, K_{xy}, K_{yx}, K_{yy} = dimensionless stiffness coefficients

$K_{mxx} = K_{xx}R/I_t\omega^2$, $K_{mxy} = K_{xy}R/I_t\omega^2$

$K_{myx} = K_{yx}R/I_t\omega^2$, $K_{myy} = K_{yy}R/I_t\omega^2$

l = length of shaft

l_k = distances to the sensors and bearings from the mass center of shaft (k=1,⋯,6)

m = mass of shaft(kg)

m_1, m_2 = shaft unbalance mass(kg)

$M_{p_{ij}}$ = dimensionless moment

P_i = dimensionless pressure(= p/p_a, i=1,2,3)

p_a = ambient pressure

r = position vector of shaft mass center

R = radius of shaft(mm)

t, T = time and dimensionless time($T = \omega t$)

$U_f = m_1 R/mC_r$, $U_m = m_2 R_2 l/2I_t C_r$

x, y = coordinate of shaft mass center

X, Y = dimensionless coordinate of shaft mass center

x_j, y_j = coordinate of j^{th} bearing(j=1, 2)

X_j, Y_j = dimensionless coordinate of j^{th} bearing

$\overline{Z}$ = dimensionless coordinate($\overline{z}/R$),

Ψ_{pi} = position of i^{th} pivot

Λ = bearing number ($=(6\mu\omega R^2)/(p_a C_r^2)$)

ω = angular speed of shaft (rad/s)

μ = viscosity of a gas

ϕ = angular coordinate in x, y plane originating from y axis

Θ_{ij} = $\theta_{ij} R/C_r$

θ_{ij} = pitch angle of a pad

1. Introduction

Conventional gas bearings have advantages such as high accuracy and low friction. However, they have the following problems: (1) vibrations due to the low stiffness and the lack of damping capability, (2) motion inaccuracy due to profile errors of axis and bearing parts. Most turbo-machine, which is operated at high speeds, such as gas turbines, jet engines, pumps and compressors, are prone to perturbing vibrations induced in the main flow of fluid-handling machines or unbalance of rotor bearing system.[1]-[3] The common causes of rotor lateral vibrations include unbalance, misalignment, rotor-to-stator rub, internal friction, loose parts, and fluid dynamic forces generated in gas bearing. Therefore, active vibration control has become an area of intense research in rotor bearing system. Significant efforts are being made to apply active vibration control(AVC) to rotating machinery in the petrochemical, aerospace and power utility industries. There are the recent works of Palazzolo, et al.[4] who proposed piezoelectric pusher as actuators for AVC of rotating machinery and Horikawa, et al.[5] who developed active static pressure air bearing.

This paper deals with synchronous vibration control of a rigid rotor using active air bearing for a high-speed turbomachinery. The authors propose a new active gas journal bearing(AGJB) which is controlled with piezoceramic[PZT] actuators. In order to suppress the synchronous vibration, it is necessary to actively control the air film pressure or the air film thickness.

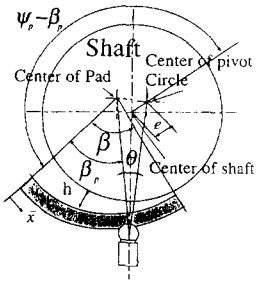

(a) Model of a pad

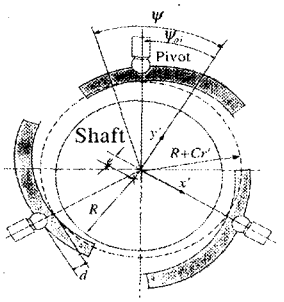

(b) Tilting-pad journal bearing

Fig. 1 Configuration of the TPGB and fluid film thickness.

To test the validity of the theoretical method, the performance of the PID control method is evaluated through simulations. The effectiveness of the PID control method is also experimentally verified by actively controlling the synchronous vibration.

2. Analysis

2.1 Basic equation and modelling

The configuration of the tilting-pad gas journal bearing(TPGB) in this paper is shown in Fig. 1. The shaft is supported without mechanical contact by three pads. A reference stationary coordinate system is selected so that the x-y plane contains the shaft center of mass. The restraint of shaft motion in the axial direction is not considered in the system. The methods of analysis used can be applied to a bearing with an arbitrary number of pads and various pivot mounting arrangements.

Figure 2 shows the configuration of the rotor bearing

system and the selected coordinate system. The shaft is assumed to be a rigid body and its motion is identified with the motion of the geometrical axis. The unbalance

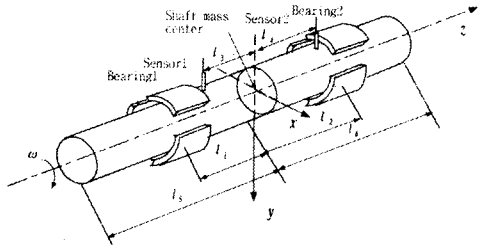

(a) Rotor bearing system

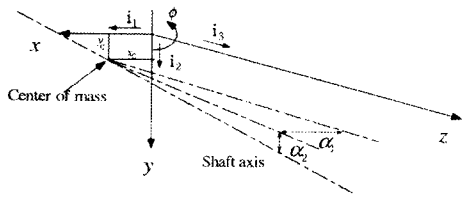

(b) Coordinate system

Fig. 2 Configuration of the rotor-bearing system and the selected coordinate system

force is caused by a point mass(m_1) attached to the surface of the shaft in the cross-sectional plane containing the center of mass, and two equal masses(m_2) attached to the surface of the shaft each at a distance ρ_u from this plane and located symmetrically in respect to the mass center. The distances to both bearings from the mass center of shaft, l_1, l_2 are 23.54mm and 26.46mm, distances to two gap sensors, l_3, l_4 are 10.84mm and 14.16mm, and to the both ends of shaft, l_5, l_6 are 90.25mm and 91.1mm.

Upon rotation, the force F_u and the moment M_u are generated at the mass center, and revolved synchronously with the shaft. The relative angle between M_u and F_u is called ϕ_u. The magnitudes of the unbalance force and moment are

$$|F_u| = Rm_1\omega^2 \quad |M_u| = 2m_2R\rho_u\omega^2 \tag{1}$$

The governing equations for the stability characteristics of the tilting-pad gas bearing system include the Reynolds' equation, which gives the pressure distribution in the gas film, as well as the equations of motion of the rotor bearing system.

Table 1 Values of parameters in the rotor-bearing system

Parameters	Value(Unit)
Shaft length	l = 181.35(mm)
Shaft mass	m = 0.28(kg)
Shaft radius	R = 8 (mm)
Bearing width	L = 15.4(mm)
Clearance	C_r = 20(μm)
Pad angular extent	β = 110 (deg)
Pivot position	β/β_p = 0.65
Dimensionless preload	0.5

Under the assumptions of laminar isothermal flow and neglecting inertial forces in the gas, the two dimensional pressure distributions satisfy the dimensionless dynamic Reynolds' equation. The components of the load force on a pad are given by:

$$f_{pi,x} = \int\int_{\Omega}(P_i - 1)\cos\phi \; d\phi d\bar{Z}$$
$$f_{pi,y} = \int\int_{\Omega}(P_i - 1)\sin\phi \; d\phi d\bar{Z} \tag{2}$$

The components of the total load force on a bearing are given by

$$f = \left(\left(\sum_{i=1}^{3} f_{pi,x'} \right) + \left(\sum_{i=1}^{3} f_{pi,y'} \right) \right)^{1/2}$$
$$\phi = \tan^{-1}\left(\left(\sum_{i=0}^{3} f_{pi,x'} \right) / \left(\sum_{i=0}^{3} f_{pi,y'} \right) \right) \tag{3}$$

Denoting the load force components in the x and y directions on the j^{th} bearing by f_{jx} and f_{jy}, they can be expressed in terms of the displacements and speeds of the shaft in the following form:

$$f_{jx} = -k_{xx}x_j - k_{xy}y_j - c_{xx}\dot{x}_j - c_{xy}\dot{y}_j$$
$$f_{jy} = -k_{yx}x_j - k_{yy}y_j - c_{yx}\dot{x}_j - c_{yy}\dot{y}_j \tag{4}$$

where x_j, y_j, $\dot{x}_j$ and $\dot{y}_j$ are the components of displacement and speed of the shaft at the cross section of the i^{th} bearing. When the time history of f_{jx} and f_{jy} is

calculated by simultaneously solving Eqs. (2) and (3), the stiffness coefficients k_{xx}, k_{xy}, k_{yx}, k_{yy} and damping coefficients c_{xx}, c_{xy}, c_{yx}, c_{yy} can be calculated from Eq. (4) by using the method of least squares

The stiffness and damping coefficients are calculated for different rotation speeds in preload 0.5 and plotted in Figs. 3 and 4. It can be found that both dimensionless stiffness coefficient K_{xx}, K_{yy} and damping coefficient C_{xx}, C_{yy} increase with the rotation speed of the shaft. The use of the eight-coefficient data helps us to understand the influence of journal bearing characteristics on the stability of the rotor system as well as the steady-state response to unbalanced system. The coefficients are also used to calculate the frequency responses of the rotary system.

2.2 Motion equation of shaft

The equations of translational motion and angular motion of the system given in Fig. 1 can be written by

$$\begin{aligned} m\ddot{x} = & -k_{xx}(x_1+x_2)-k_{xy}(y_1+y_2)-c_{xx}(\dot{x}_1+\dot{x}_2) \\ & -c_{yx}(\dot{y}_1+\dot{y}_2)+m_1R\omega^2\cos\omega t \\ m\ddot{y} = & -k_{xy}(x_1+x_2)-k_{yy}(y_1+y_2)-c_{xy}(\dot{x}_1+\dot{x}_2) \\ & -c_{yy}(\dot{y}_1+\dot{y}_2)+m_1R\omega^2\sin\omega t \end{aligned} \tag{5}$$

$$\begin{aligned} I_t\,\ddot{\alpha}_1+I_p\omega\dot{\alpha}_2 = & \; k_{xx}(x_2l_2-x_1l_1)+k_{xy}(y_2l_2-y_1l_1) \\ & +c_{xx}(\dot{x}_2l_2-\dot{x}_1l_1)+c_{yy}(\dot{y}_2l_2-\dot{y}_1l_1) \\ & +\frac{m_2R\omega^2l}{2}\sin(\omega t-\phi_u) \\ -I_t\,\ddot{\alpha}_2+I_p\omega\dot{\alpha}_2 = & -k_{xx}(x_2l_2-x_1l_1)-k_{xy}(y_2l_2-y_1l_1) \\ & -c_{xx}(\dot{x}_2l_2-\dot{x}_1l_1)-c_{yy}(\dot{y}_2l_2-\dot{y}_1l_1) \\ & +\frac{m_2R\omega^2l}{2}\sin(\omega t-\phi_u) \\ I_p\dot{\omega} = & \; 0 \end{aligned} \tag{6}$$

After nondimensionalization, Eqs. (5) and (6) may be written as

$$[\ddot{V}]+[C][\dot{V}]+[K][V]=A\cos T+B\sin T \tag{7}$$

where, $V=[X\ A_1\ Y\ A_2]^T$

$$\{A\}=[\ U_f\ -U_m\sin\phi_u\quad 0\ -U_m\cos\phi_u\ ]$$

$$\{B\}=[\ 0\quad U_m\cos\phi_u\quad U_f\quad -U_m\sin\phi_u\ ]$$

$$[K]=\begin{bmatrix} 2K_{xx} & \frac{l_2-l_1}{R}K_{xx} & 2K_{xy} & \frac{l_2-l_1}{R}K_{xy} \\ (l_2-l_1)K_{mxx} & \frac{l_2^2+l_1^2}{R}K_{mxx} & (l_2-l_1)K_{mxy} & \frac{l_2^2+l_1^2}{R}K_{mxy} \\ 2K_{yx} & \frac{l_2-l_1}{R}K_{yx} & 2K_{yy} & \frac{l_2-l_1}{R}K_{yy} \\ (l_2-l_1)K_{myx} & \frac{l_2^2+l_1^2}{R}K_{myx} & (l_2-l_1)K_{myy} & \frac{l_2^2+l_1^2}{R}K_{myy} \end{bmatrix}$$

$$[C]=\begin{bmatrix} 2C_{xx} & \frac{l_2-l_1}{R}C_{xx} & 2C_{xy} & \frac{l_2-l_1}{R}C_{xy} \\ (l_2-l_1)C_{mxx} & \frac{l_2^2+l_1^2}{R}C_{mxx} & (l_2-l_1)C_{mxy} & \frac{l_2^2+l_1^2}{R}C_{mxy}+G \\ 2C_{yx} & \frac{l_2-l_1}{R}C_{yx} & 2C_{yy} & \frac{l_2-l_1}{R}C_{yy} \\ (l_2-l_1)C_{myx} & \frac{l_2^2+l_1^2}{R}C_{myx}-G & (l_2-l_1)C_{myy} & \frac{l_2^2+l_1^2}{R}C_{myy} \end{bmatrix}$$

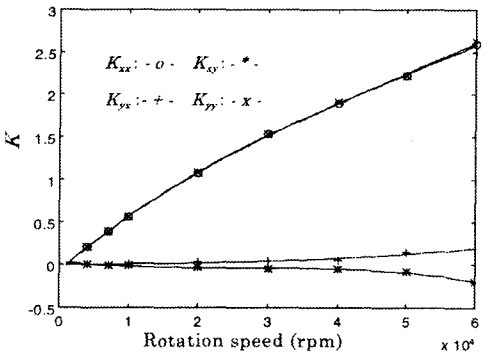

Fig. 3 Dimensionless K coefficients

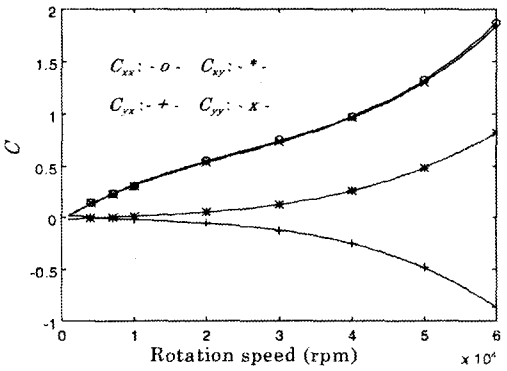

Fig. 4 Dimensionless C coefficients

Here $[C]$ and $[K]$ are the dimensionless damping and stiffness matrices, respectively. In general, they are asymmetric matrices, which reflect gyroscopic moments, internal and external damping terms, and asymmetric

bearing properties.

The rotor bearing system has two rigid modes: a parallel mode and a conical mode. Figure 5 shows the relationship between turbine shaft vibration and rotation speed. The analytical predictions of the shaft rotation speeds at which modal vibration becomes large are 11,760rpm and 35,000rpm. These values are in good agreement with the experimental results. The amplitude of unbalance-excited vibration depends mainly on the size of the unbalance. When the frequency of shaft rotation equals the natural frequency of a rigid mode, the amplitude of the shaft becomes larger due to resonance.

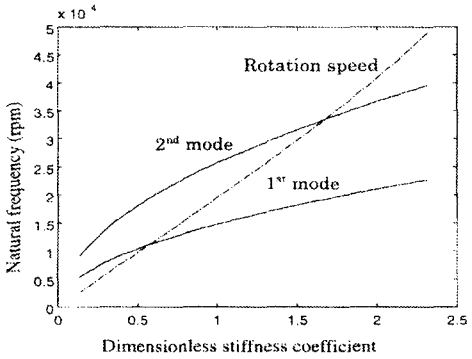

Fig. 5 Resonance frequency of 1st and 2nd rigid mode

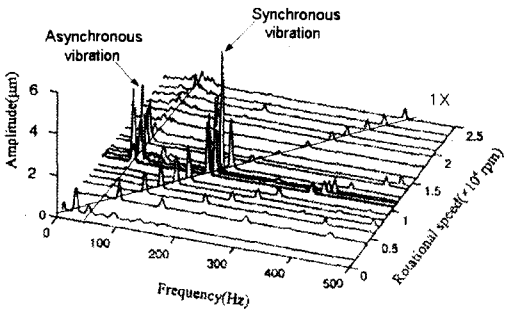

Fig. 6 Waterfall chart of frequency response of turbine shaft at UL position of gap sensor. (Experimental result)

The waterfall charts of frequency spectrum of the turbine shaft at UL locations are shown in Fig. 6. At low rotating speeds, these vibrations are stable so that an impulse perturbation of the rotor causes a short time transient vibration process. In this range of the rotating speed, the rotor behaves as a rigid body. When the rotating speed approaches the machine's first unbalance resonance, the 1X vibration amplitudes start increasing as shown in Fig. 6. The rotating unbalance force pushes the journal to the side of the bearing, resulting in high dynamic eccentricity. In order to suppress the unstable vibration which appears when the rotation speed exceeds the critical speed, some of the geometrical or physical parameters of the bearing should be controlled actively.

3. Controller Design

The equations of motion in Eq. (7) may be written in standard state-space form as

$$\begin{aligned} \dot{\overline{X}}(T) &= A \cdot \overline{X}(T) + B_1 \cdot u(T) + B_2 \cdot w(T) \\ \overline{Y}(T) &= C \cdot \overline{X}(T) + D \cdot u(T) \end{aligned} \tag{8}$$

where, $\overline{X}(T) = [X\ A_1\ Y\ A_2\ \dot{X}\ \dot{A}_1\ \dot{Y}\ \dot{A}_2]$,
$\overline{Y}(T) = [X_3\ X_4\ Y_3\ Y_4]$,

$$A = \begin{bmatrix} O_{4\times4} & I_{4\times4} \\ -K_{4\times4} & -C_{4\times4} \end{bmatrix}, \qquad B_2 = \begin{bmatrix} O_{4\times4} \\ I_{4\times4} \end{bmatrix},$$

$$B_1 = \begin{bmatrix} & K_{xx} & -K_{mxx}l_1 & 0 & 0 \\ 0_{4\times4} & -K_{xx}\sin\alpha & -K_{mxx}l_1\sin\alpha & -K_{yy}\cos\alpha & K_{myy}l_1\cos\alpha \\ & K_{xx} & -K_{mxx}l_2 & 0 & 0 \\ & -K_{xx}\sin\alpha & -K_{mxx}l_2\sin\alpha & -K_{yy}\cos\alpha & -K_{myy}l_2\cos\alpha \end{bmatrix}$$

$$C = \begin{bmatrix} 1 & -l_3/R & 0 & 0 & 0 & 0 & 0 & 0 \\ 1 & -l_4/R & 0 & 0 & 0 & 0 & 0 & 0 \\ 1 & 0 & 1 & -l_3/R & 0 & 0 & 0 & 0 \\ 1 & 0 & 1 & -l_4/R & 0 & 0 & 0 & 0 \end{bmatrix}, \tag{9}$$

$$D = \begin{bmatrix} 0 & 0 & 0 & 0 \\ 0 & 0 & 0 & 0 \\ 0 & 0 & 0 & 0 \\ 0 & 0 & 0 & 0 \end{bmatrix}, \quad w(T) = \begin{bmatrix} U_f\cos(T) \\ U_m\sin(T-\phi_u) \\ U_f\sin(T) \\ -U_m\cos(T-\phi_u) \end{bmatrix}$$

In there equations, X is the state vector, Y is the measured output. u is the control input and w is the disturbance input. The control inputs u_{ij}, u_{ij} are the commanded displacements of the pads. A simplified axis dynamic model in the y direction is shown in Fig. 7. The control forces are produced by a tilting-pad journal bearing consisting of three pads with two PZT actuators.

4. Experiments for vibration control

An experiment on the vibration control of a

high-speed turbomachinery using two active gas bearing has been performed. The basic design of an active gas journal bearing (AGJB) used in this paper is shown in Fig. 7. This figure shows two tilting-pad journal bearings each of which consists of one pad without PZT actuator and two pads with PZT actuators.

In the active pad, a PZT actuator of stack type is used for controlling floating characteristics. Pivots containing piezoelectric actuators support the pads and by applying voltage to the actuators can actively control their radial position. The values of parameters used in the gas expander are shown in Table 2. A PZT actuator is inserted between the body and each active pad, forming a noncontact actuator, which drives the shaft in the x or y direction through the pressurized gas film (gas film thickness: 20 μm)

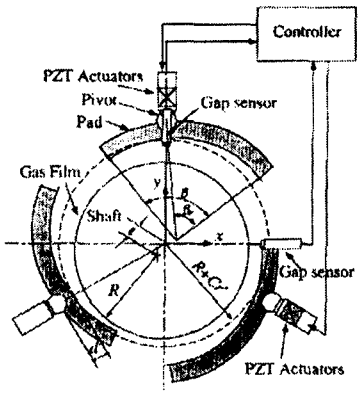

Fig. 7 Configuration of AGJB

Table 2 Values of parameters in gas expander

Parameters	Value(Unit)
Turbine inlet pressure	0.5 ~ 5 Kgf/cm^2
Turbine outlet pressure	0 ~ 1.2 Kgf/cm^2
Thrust bearing	Externally Pressurized Thrust Bearing EPTB)
Radial bearing	Tilting Pad Gas Bearing TPGB)
Inlet flow rate	10 ~ 45 Nm^3/h
Fluid	Air
Pivot position	β/β_p= 0.65
Dimensionless preload	0.5

Figure 8 shows the schematic diagram of the turbine expander for the active control system. Four displacements, measured by four gap sensors in the radial direction, are input to the controller board (dSPACE Co. 1103) through an A/D converter. Two-control input made by DSP is supplied to two active pads as actuators through the D/A converter and power amplifiers. The radial direction of the shaft was controlled by each DSP. The sampling time was set to be 0.1msec(sampling frequency 10 kHz). Namely, the four radial axis are controlled by only one chip DSP.

We investigated the unstable vibration suppression performance by changing gain of the feedback control of the control force. Figure 9 shows the block diagram of the rotor-bearing system of the active control.

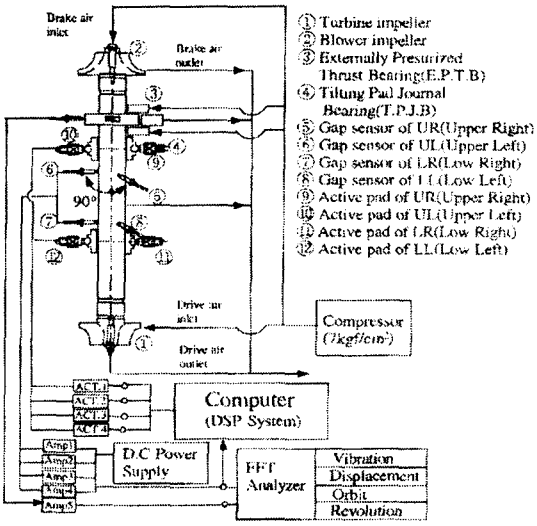

Fig. 8 Schematic diagram of the turbine expander for active control system

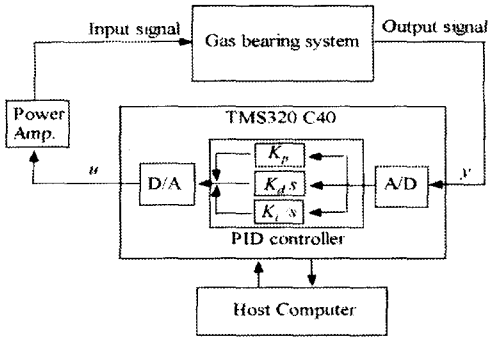

Fig. 9 Schematic diagram of the rotor bearing system of active control system

In a PID controller, the control action is generated as a sum of three terms. The PID control law is thus described as

$$\frac{U(s)}{Y(s)} = K_p + K_d s + \frac{K_i}{s} = K_p\left(1 + T_d s + \frac{1}{T_i s}\right) \quad (10)$$

where $Y(s)$: sensor output, $U(s)$: control input, T_i : integral time, T_d : derivative time, K_p : proportional gain, K_i : integral gain, K_d : derivative gain.

The performance of the PID controller is evaluated through simulations to check its applicability to suppression of unbalance response or reduction of unbalance force in AGJB system. The synchronous vibration control has been performed using the PID control method. Several controllers have been tested with various proportional and derivative gains: K_p and K_d. However, the integral gain has been held to be the same value(K_i=0.001), because the effect of the integral gain K_i on the control performance is negligible.

5. Discussion and Results

In this section, we examine the operation of the gas bearing system using PID controller when the rotor is subjected to external periodic disturbances. In these simulations, the displacement of the shaft in the x-direction at the two bearing locations is examined. The control of the x, y-direction displacement of the bearing pads is achieved by piezoelectric actuators.

The performance of control at a rotating speed of 11,760 rpm is shown in Figs. 10~12. Figure 10 shows the simulation result of the shaft displacement response at the bearings and the control inputs when PID controller is applied. The amplitude of vibration is reduced by about 60% in a few cycles after control input is applied. A significant reduction of vibration is achieved with the PID controller.

Figure 11, 12 shows the experimental result of the shaft displacement Lissajous response at the each bearings when PID controller is applied. Hence, the synchronous vibration of a rotor bearing system was effectively suppressed by using output feedback of the designed PID controller as it can also be observed in the experimental response. The Amplitude of synchronous vibration was reduced by 61.5% and it was also in matching the simulation result.

Figure 13 shows the peak changes of power spectra of the corresponding gap sensor signals due to the gain K_p increment. The peak frequency of synchronous vibration was observed to be 196 Hz. The integral and derivative gains were set to be 0.001, 0.01, respectively. The closed loop behaviors have been monitored as the proportional gain K_p which successively increased. When the K_p is 150, optimal performance can be obtained. At UL, UR gap sensor position, the overall control effectiveness is observed such that the peak of UL, UR gap sensor is decreased by 10 dB and UL, UR gap sensor is 7dB when PID controller is applied.

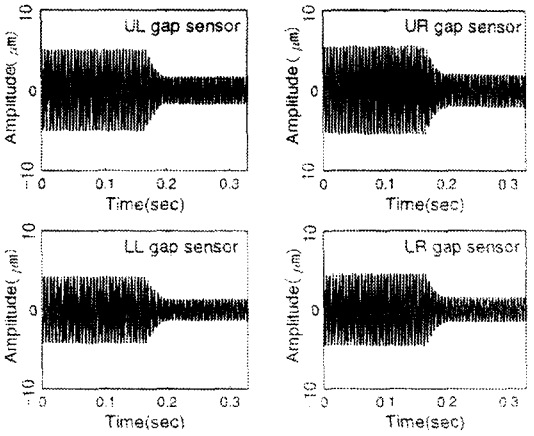

Fig. 10 Time response of the shaft with PID controller (Simulation).

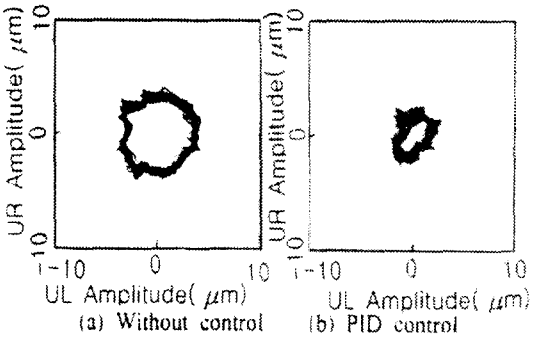

(a) Without control (b) PID control

Fig. 11 Rresponse of shaft orbits at 11,760 rpm (Experiment).

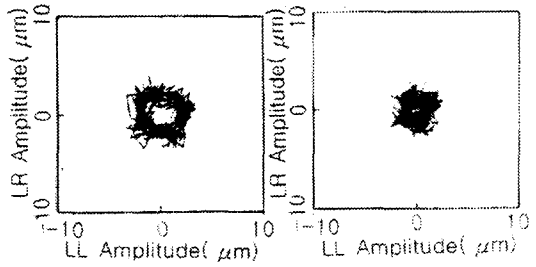

(a) Without control (b) PID control

Fig. 12 Response of shaft orbits at 11,760 rpm (Experiment).

6. Conclusion

A new active gas journal bearing system has been proposed in this study in order to control the synchronous vibration of the rotor bearing system. Active pads are actuated by a stack type piezoelectric actuator.

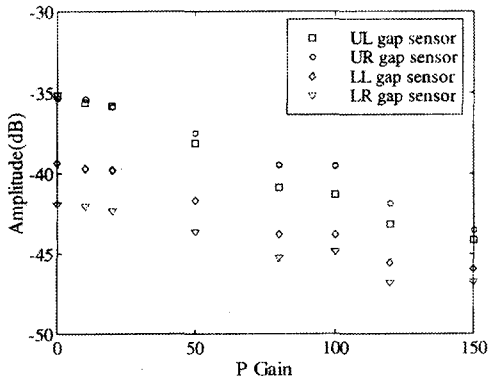

Fig. 13 Peak changes of power spectra of the gap sensor signals due to the gain K_p increment

At first, the vibration characteristics of the journal bearing system were investigated. The synchronous vibration occurred around a frequency of 196Hz. In order to control synchronous vibration, PID controllers have been applied. With the proper selection of gains, the synchronous vibration could be suppressed. It was also observed that too large gains caused excessive vibration at other frequencies. The experimental results show the effectiveness of the control system for suppressing the unbalanced response of the rigid modes. This results obtained here are reasonable and encouraging for future studies on AGJB system.

References

1. Eusepi M. W., and Wilcock D. F., "A New Hydrodynamic Gas Bearing Concept," Transactions of the ASME, Vol. 110, pp. 614-620, 1988.
2. Heshmat H., "Advancements in the Performance of Aerodynamic Foil Journal Bearing: High Speed and Load Capability," J. of Tribology, Vol. 116, pp. 287-294, 1994.
3. Garner D. R., Lee C. S., and Martin F. A., "Stability of Profile Bore Bearings : Influence of Bearing Type Selection," Tribology International, Vol.13, pp. 204-210, 1980.
4. A. B. Palazzolo, et al, "Hybrid Active Vibration Control of Rotor Bearing Systems Using Piezo -actuator," J. of Vibration and Acoustics., Vol. 135, pp. 105-111, 1993.
5. Horikawa, and A. Shimokohbe, "An Active Air Bearing," JSME, Int. Journal, Vol. 33, No. 1, pp. 55-60, 1990.
6. T. K. Kwon, J. H. Qiu, and J. J. Tani, "Control of Self-Excited Vibrations of a Rotor System with Active Gas Bearing," J. of JSME, Vol. 66 No. 643, pp. 724-730, 2000.